The Astrophysical Journal, 607:904–912, 2004 June 1

CHANDRA OBSERVATION OF THE TRIFID NEBULA: X-RAY EMISSION FROM THE O STAR COMPLEX AND ACTIVELY FORMING PRE–MAIN-SEQUENCE STARS

Jeonghee Rho and Solange V. Ramírez
Spitzer Science Center, MS 220-06, California Institute of Technology, Pasadena, CA 91125

Michael F. Corcoran[1] and Kenji Hamaguchi
NASA Goddard Space Flight Center, Code 662, Greenbelt, MD 20771

and

Bertrand Lefloch
Laboratoire d'Astrophysique, Observatoire de Grenoble, BP 53, F-38041 Grenoble Cedex 9, France
Received 2003 October 23; accepted 2004 January 21

ABSTRACT

The Trifid Nebula, a young star-forming H II region, was observed for 16 hr by the ACIS-I detector on board the *Chandra X-Ray Observatory*. We detected 304 X-ray sources, 30% of which are hard sources and 70% of which have near-infrared counterparts. *Chandra* resolved the HD 164492 multiple system into a number of discrete X-ray sources. X-ray emission is detected from components HD 164492A (an O7.5 III star that ionizes the nebula), B and C (a B6 V star), and possibly D (a Be star). Component C is blended with an unidentified source to the northwest. HD 164492A has a soft spectrum ($kT \approx 0.5$ keV), while the component C blend shows much harder emission ($kT \approx 6$ keV). This blend and other hard sources are responsible for the hard emission and Fe K line seen by *ASCA*, which was previously attributed entirely to HD 164492A. The soft spectrum of the O star is similar to emission seen from other single O stars and is probably produced by shocks within its massive stellar wind. Lack of hard emission suggests that neither a magnetically confined wind shock nor colliding wind emission is important in HD 164492A. A dozen stars are found to have flares in the field, and most of them are pre–main-sequence stars (PMS). Six sources with flares have both optical and Two Micron All Sky Survey counterparts. These counterparts are not embedded, and thus it is likely that these sources are in a later stage of PMS evolution, possibly Class II or III. Two flare sources did not have any near-IR, optical, or radio counterparts. We suggest that these X-ray flare stars are in an early PMS stage (Class I or earlier). We also detected X-ray sources apparently associated with two massive star-forming cores, TC 1 and TC 4. The spectra of these sources show high extinction and X-ray luminosities of $(2–5) \times 10^{31}$ ergs s^{-1}. If these sources are Class 0 objects, it is unclear whether their X-ray emission is due to solar-type magnetic activities, as in Class I objects, or to some other mechanism.

Subject headings: ISM: individual (Trifid Nebula) — stars: activity — stars: pre–main-sequence — X-rays: stars

On-line material: machine-readable table

1. INTRODUCTION

Despite the fact that X-ray observations of star-forming regions have been a powerful tool for discovering young stellar objects (YSO) and T Tauri stars (TTS) since *Einstein* (Feigelson & Montmerle 1999 and references therein), long-wavelength (IR and submillimeter) emission is used to define evolutionary classes for young stars. Classes I–III are solely based on the excess seen in the IR spectral energy distribution (SED) with respect to stellar blackbody photospheric emission, as measured by the spectral index $\alpha_{\rm IR} = d \log (\lambda F_\lambda)/d \log \lambda$ between $\lambda = 2.2$ and 10–25 μm; Class I, II, and III correspond to $\alpha_{\rm IR} > 0$, $-2 < \alpha_{\rm IR} < 0$, and $\alpha_{\rm IR} < -2$ (Lada 1987). Class 0 stars represent the earliest phase of star formation, identified by the ratio of submillimeter to bolometric luminosity (André, Ward-Thompson, & Barsony 1993), and are seen as condensations in submillimeter far-infrared dust continuum maps; these condensations often show collimated CO outflows or internal heating sources. X-ray–bright T Tauri stars usually belong to either Class II or III.

High-resolution images obtained by the *Chandra X-Ray Observatory* open a new era in the study of star formation because the 1″ resolution of *Chandra* is necessary to resolve individual sources in nearby star-forming regions, and because confusion due to foreground and background stars is much less important at X-ray energies than in the optical and near-infrared regime. Recent *Chandra* observations of Orion (Garmire et al. 2000; Feigelson et al. 2002) detected hundreds of X-ray sources, e.g., pre–main-sequence stars (PMS) with masses in the range 0.05–50 $M_\odot$, and a combined infrared and X-ray study suggests that the X-ray luminosity of PMS stars depends on stellar mass, rotational history, and magnetic field (Garmire et al. 2000). A high percentage of Class I PMS stars were also found to be X-ray emitters; in ρ Oph, 70% of identified Class I stars are X-ray–bright. Strong X-ray flares from PMS stars in ρ Oph (Imanishi, Koyama, & Tsuboi 2001), Monoceros R2 (Kohno, Koyama, & Hamaguchi 2002), and Orion (Feigelson et al. 2002) were detected from Class I, II, and III objects, possibly because of magnetic activity. Moreover, X-ray emission from Class 0 candidates was detected in OMC-3 (Tsuboi et al. 2001).

The Trifid Nebula (M20) is one of the best-known astrophysical objects. It is a classical nebula ionized by an O7.5

[1] Universities Space Research Association, 7501 Forbes Boulevard, Suite 206, Seabrook, MD 20706.

star, HD 164492A, and the ionized nebula glows in red light. The nebula is trisected by obscuring dust lanes, giving the Trifid its name. A blue reflection nebula appears to the north of the red nebula. At an age of $\sim 3 \times 10^5$ yr, the Trifid is a young H II region. Recent studies using the *Infrared Space Observatory* (*ISO*) and the *Hubble Space Telescope* (*HST*) (Cernicharo et al. 1998; Lefloch & Cernicharo 2000; Hester et al. 1999) show the Trifid to be a dynamic, "pre-Orion" star-forming region containing young stars undergoing episodes of violent mass ejection, with protostars like HH 399 (Lefloch et al. 2002) losing mass and energy to the nebula in optically bright jets. Four massive (17–60 $M_\odot$) protostellar cores were discovered in the Trifid from millimeter wave observations. These cores are associated with molecular gas condensations at the edges of clouds (Lefloch & Cernicharo 2000). T Tauri stars and young stellar object candidates were also identified using near-infrared color-color diagrams from the Two Micron All Sky Survey (2MASS) data (Rho et al. 2001). Unlike better studied nearby star-forming regions such as Orion and ρ Oph, star-forming activities in the Trifid have only recently been recognized (Cernicharo et al. 1998), and as a result of this (and also due to contamination by foreground and background stars in the optical and IR), the population of PMS stars in the Trifid has not been fully investigated. The distance to the Trifid Nebula is between 1.68 and 2.84 kpc (Lynds & O'Neil 1985; Kohoutek, Mayer, & Lorenz 1999 and references therein), and a distance of 1.68 kpc is adopted in this paper.

In this paper, we report results of *Chandra* observations of the Trifid Nebula. *Chandra* resolved the HD 164492 multiple system into a number of discrete X-ray sources, and we present their X-ray properties, which include components A (an O star), C (a B6 V star), and B (an A2 Ia star). Our *Chandra* observations revealed 304 sources, and we found that 30% of the sources have hard emission similar to that from PMS stars. Among these candidate PMS stars, we report properties of about a dozen flare sources, which include unusual variability from the O star and unusual emission from an A-type supergiant. We also discuss the X-ray properties of the HD 164492 complex, the properties of X-ray sources that are apparently associated with two protostellar cores, and also the properties of some apparently strongly variable objects.

2. OBSERVATIONS

The Trifid Nebula was observed with the Advanced CCD Imaging Spectrometer (ACIS) detector on board *Chandra* (Weisskopf et al. 2002) on 2002 June 13. The results presented here arise from the imaging array (ACIS-I), which consists of four 1024×1024 front-side illuminated CCDs. The array was centered at R.A. $= 18^{\rm h}02^{\rm m}28^{\rm s}$ and decl. $= -22^\circ 56' 50''$ (J2000.0) and covered an area in the sky of about $17' \times 17'$. The total exposure time of the ACIS observations was 58 ks. This observation is sensitive to X-ray luminosities of 5×10^{29} ergs s^{-1}, assuming an appropriate PMS X-ray spectrum (temperature of 1 keV and an absorption 1.6×10^{21} cm^{-1}) at the distance (1.68 kpc) of the Trifid.

We began data analysis with the Level 1 processed event list provided by the pipeline processing at the *Chandra* X-Ray Center. The energy and grade of each data event were corrected for charge transfer inefficiency (CTI), applying the algorithm described by Townsley et al. (2000). The event file was filtered to include event grades of 0, 2, 3, 4, and 6, and filtered by time intervals to exclude background flaring intervals or other bad times. The filtering process was done using the *Chandra* Interactive Analysis of Observations (CIAO) package,[2] provided by the *Chandra* X-ray Center.

Figure 1 shows the *Chandra* ACIS-I three-color image of the Trifid. Hundreds of point sources are detected with little diffuse emission. X-ray sources were located using the *wavdetect* tool within the CIAO package. This tool performs a Mexican hat wavelet decomposition and reconstruction of the image after accounting for the spatially varying point-spread function as described by Freeman et al. (2002). We used wavelet scales ranging from 1 to 16 pixels in steps of $\sqrt{2}$ and a default source threshold probability of 1×10^{-6}. The *wavdetect* tool was run using an exposure map, and it produced a catalog of 353 sources from the entire ACIS-I field of view (FOV). Then we identified false sources produced by cosmic rays or cases in which the source counts are below the background counts. This observation finally resulted in 304 X-ray sources detected from the total ACIS-I FOV ($17' \times 17'$). The full source list is given in Table 1 in order of right ascension (R.A.); 30% of these sources are shown to be hard (Fig. 1, *blue*). The hard sources have a spectral hardness ratio (SHR) greater than -0.2, where SHR is the ratio of the net counts in the hard 2.0–8.0 keV band to those in the soft 0.5–2.0 keV band. Diffuse emission was not obvious in the *Chandra* images of the Trifid Nebula with our current data processing. Nondetection of diffuse emission in M20 is consistent with a claim that high-mass star-forming regions without stars earlier than O6 may be unlikely to exhibit diffuse soft X-rays (Townsley et al. 2003; Abbott 1982).

The brightest source in the field corresponds to the O star HD 164492A (source 102) and has 884 counts. This is equivalent to 0.047 photons per frame, which is small enough so as not to be affected by pileup effects (the pileup fraction is $\ll 0.05$). In order to verify the hard emission and Fe K line detected in the *ASCA* spectra of HD 164492A (Rho et al. 2001), we extracted a spectrum using the same extraction region that was used in the *ASCA* analysis and confirmed that the *Chandra* and *ASCA* spectra are the same within the errors. However, we found that HD 164492A is actually a soft source (see § 6 for details), while the hard emission and Fe K line (which were attributed to the O star in the *ASCA* analysis) is actually produced by the hard sources resolved by *Chandra*, as shown Figure 2. In addition, the emission previously attributed entirely to HD 164492A in an analysis of *ROSAT* PSPC data (Rho et al. 2001) is now resolved into a dozen X-ray sources, as shown in Figures 1 and 2.

To confirm the X-ray astrometry, we used the 2MASS[3] final release point-source catalog to search for near-IR counterparts to the X-ray sources in the full source list. We cross-correlated the positions of the 2MASS sources with the positions of our X-ray sources. Within $5'$ of the *Chandra* aim point, we found 72 2MASS sources that coincide with X-ray source positions. We computed the total R.A. and decl. offset of these sources and obtained offsets of $-0''.16$ in R.A., and $-0''.09$ in decl., which are less than one-third of a pixel. Therefore, the astrometry of the Trifid ACIS image was confirmed with the minor systematic errors in the *Chandra* aspect solution.

3. THE MULTIPLE SYSTEM HD 164492

The HD 164492 complex is a multiple stellar system composed of seven physically related components, A–G

[2] Additional information on CIAO is available at http://cxc.harvard.edu/ciao/index.html.

[3] Additional information on 2MASS is available at http://www.ipac.caltech.edu/2mass.

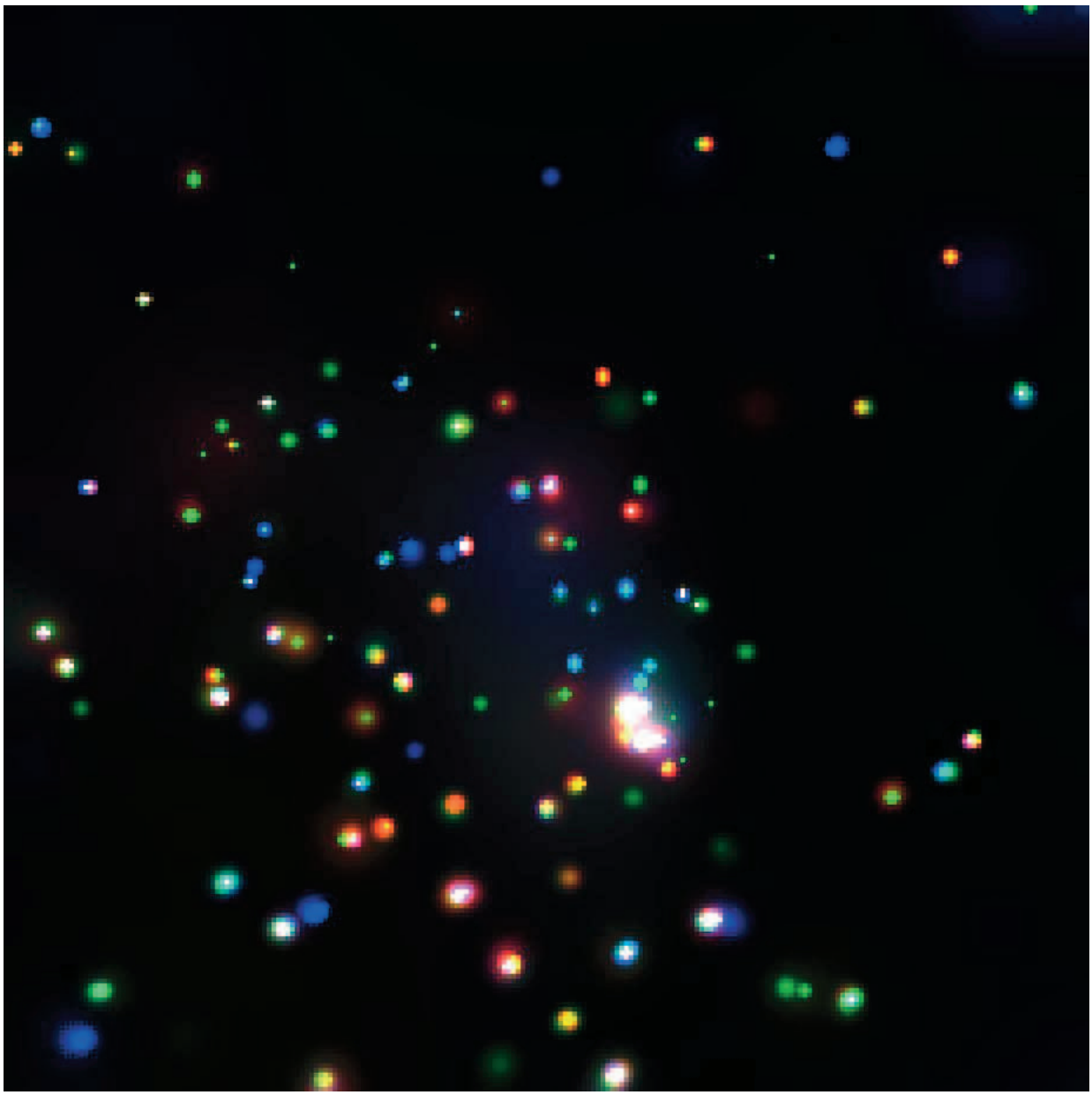

FIG. 1.—Three-color *Chandra* ACIS-I image of the Trifid Nebula: 0.5–1 (*red*), 1–2 (*green*), and 2–8 keV (*blue*). The image is centered at R.A. = $18^{h}02^{m}26^{s}$ and decl. = $-23^{\circ}00'39''$ (J2000.0) and covers a 7.′5 field of view.

(Kohoutek et al. 1999). Component HD 164492A is the O7.5 III((f)) star responsible for ionizing the nebula. This complex was observed as an unresolved bright X-ray source in *ROSAT* PSPC images (Rho et al. 2001). Our *Chandra* images (Figs. 1 and 2) resolve this complex into a number of discrete X-ray sources. X-ray emission is clearly detected from components A, B, and C, as shown in Table 2 (Fig. 2). HD 164492A is the brightest X-ray source in this complex. Component HD 164492C (a B6 V star; Gahm, Ahlin, & Lindroos 1983) is a bright X-ray source (source 94) and is barely resolved from a nearby X-ray source northwest of C (source 91), which has no obvious optical counterpart (Fig. 2). Source D (a Be star) is a strong Hα emitter (Herbig 1957) and has a disk (resolved by a radio image) similar to proplyds in the Orion nebula (O'Dell 2001). Component D is much fainter in X-rays than component C.

3.1. *HD 164492A*

The X-ray light curve of the HD 164492A shows small but significant variability ($\sim$20% in the 10 hr observation; Fig. 4). This is unusual, since most OB stars are not known X-ray variables. X-ray variability is not widely known from early-type stars based on previous *Einstein* and *ROSAT* surveys (Chlebowski, Harnden, & Sciortino 1989; Berghöfer, Schmitt, & Cassinelli 1996). However, recent *Chandra* observations show significant variability from some early-type stars (Feigelson et al. 2002). For example, θ^2 Ori A, an O9.5 star, shows a 50% drop in 10 hr with multiple 10%–20% flares (Feigelson et al. 2002). Some level of time variability is also observed from other early-type stars in Orion (Schulz et al. 2001). The spectrum of the O star shows thermal emission, as shown in Figure 3*a*. We fitted the X-ray spectra of

TABLE 1
CATALOG OF X-RAY SOURCES

NUMBER	WAVELET ID	CXO M20 (R.A.)	CXO M20 (decl.)	NET COUNTS (counts ks^{-1})	S/N	HARDNESS RATIO
1.....	177	18 01 50.61	22 54 39.6	12 ± 4	3	-0.23 ± 0.20
2.....	208	18 01 50.79	22 52 18.5	22 ± 7	3	0.09 ± 0.13
3.....	206	18 01 52.54	22 57 33.6	22 ± 6	4	-0.26 ± 0.16
4.....	207	18 01 53.57	22 51 35.6	24 ± 7	4	0.56 ± 0.16
5.....	333	18 01 57.18	23 01 22.1	58 ± 9	11	-0.49 ± 0.14
6.....	344	18 01 57.64	23 00 01.7	13 ± 4	3	-0.19 ± 0.20
7.....	197	18 01 58.33	22 52 26.5	21 ± 6	5	-0.36 ± 0.14
8.....	196	18 01 59.07	22 52 27.5	73 ± 10	12	-0.49 ± 0.11
9.....	352	18 01 59.12	23 00 55.3	20 ± 5	5	0.76 ± 0.22
10.....	195	18 01 59.85	22 53 14.8	41 ± 7	9	-0.62 ± 0.16

NOTES.—Table 1 is published in its entirety in the electronic edition of the *Astrophysical Journal*. A portion is shown here for guidance regarding its form and content. Units of right ascension are hours, minutes, and seconds, and units of declination are degrees, arcminutes, and arcseconds.

HD 164492A using two collisional ionization equilibrium thermal models (a Mewe-Kaastra plasma model: Kaastra 1992; and an updated Raymond-Smith model: Raymond & Smith 1977; MEKAL and APEC in XSPEC). Both models gave similar results. We assumed subsolar metal abundance (0.3 solar); assuming solar abundances produced less than a 20% change in the derived spectral parameters. The best fit of the spectrum of the O star yields $N_{\rm H} = 1(<5) \times 10^{21}$ cm^{-2} and a temperature of $kT_s = 0.5(<0.6)$ keV, which implies an X-ray luminosity of 2.8×10^{31} ergs s^{-1}. The derived temperature is

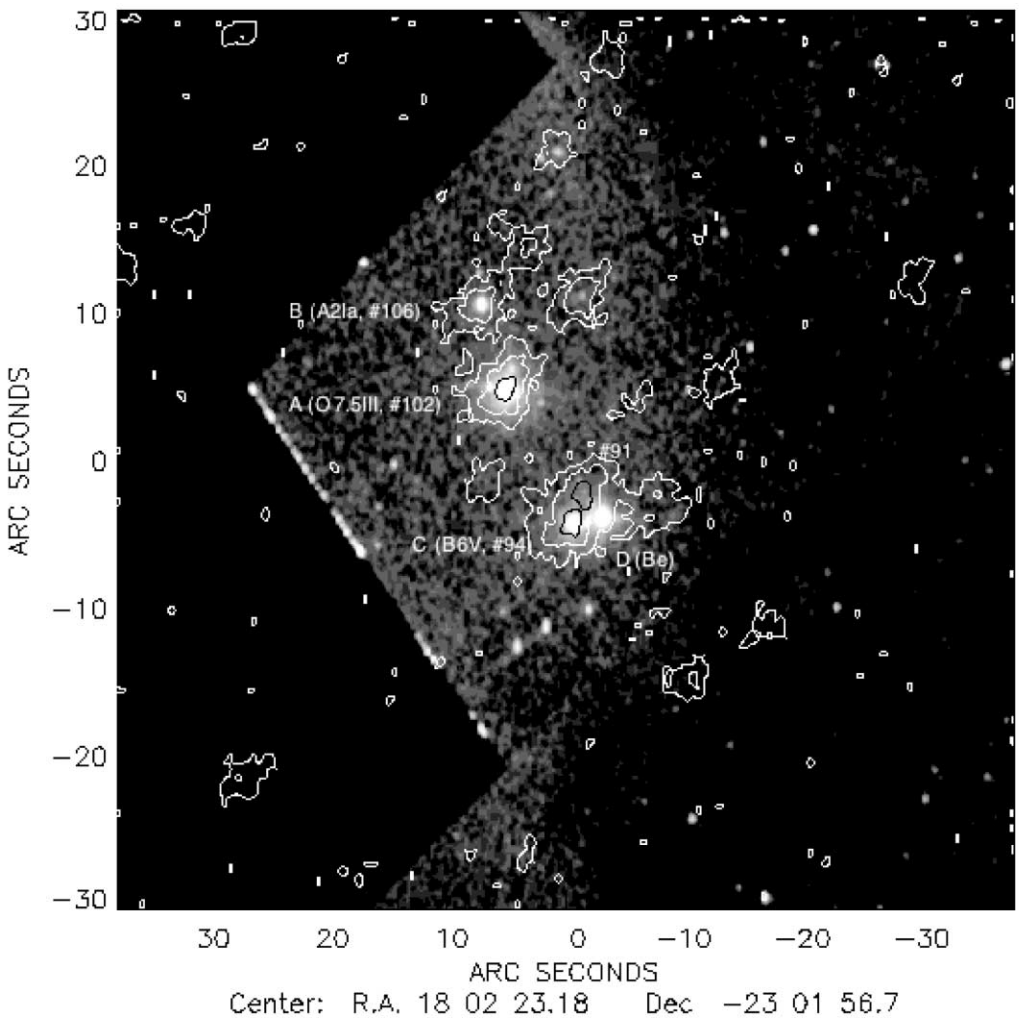

FIG. 2.—Sources in the HD 164492 complex. The gray-scale image of *HST* superposed on *Chandra* X-ray contours. The components of HD 164492 are marked.

TABLE 2

SUMMARY OF SELECTED X-RAY SOURCES

NUMBER[a]	WAVELET ID[a]	CXO M20 R.A.	CXO M20 Decl.	NET[b]	S/N[b]	MAXIMUM (counts ks^{-1})[c]	MINIMUM (counts ks^{-1})[c]	RATIO[c]	PROBABILITY OF CONSTANCY (%)[d]	HARDNESS RATIO[e]	2MASS[f]	OPTICAL[g]	L_X (10^{31})
8.....	196	18 01 59.07	22 52 27.4	73	12	5.87 ± 2.26	1.44 ± 0.34	4.07 ± 1.84	55	-0.49 ± 0.11	Y	[Y]	0.32
23.....	173	18 02 07.77	22 55 33.8	58	19	5.52 ± 2.09	0.95 ± 0.28	5.79 ± 2.77	4	-0.58 ± 0.15	TTS	[Y]	0.27
38 (TC 4).....	347	18 02 12.47	23 05 48.0	62	9	2.34 ± 1.92	1.06 ± 0.35	2.21 ± 1.96	100	0.67 ± 0.13	Y?	N	1.9
91 (C2).....	235	18 02 23.05	23 01 58.1	857	129	15.99 ± 3.05	9.72 ± 0.52	1.65 ± 0.33	2	-0.47 ± 0.03	N	N	6[h]
94 (CD).....	234	18 02 23.16	23 02 00.2	831	119	15.19 ± 2.99	6.79 ± 2.22	2.24 ± 0.85	79	-0.50 ± 0.03	Y	[Y]	14[h]
97.....	272	18 02 23.25	23 01 34.9	48	12	3.15 ± 1.76	1.03 ± 0.29	3.06 ± 1.91	8	-0.18 ± 0.13	YSO	N	0.22
102 (A).....	230	18 02 23.54	23 01 50.9	884	114	19.95 ± 3.34	9.88 ± 3.89	2.02 ± 0.87	46	-0.89 ± 0.04	Y	[Y]	2
106 (B).....	229	18 02 23.71	23 01 45.4	299	47	8.34 ± 2.40	3.15 ± 1.76	2.65 ± 1.67	100	-0.64 ± 0.07	Y	Y	5
117 (TC 1).....	264	18 02 25.16	23 01 26.7	41	15	2.37 ± 1.63	0.69 ± 0.27	3.44 ± 2.72	100	0.24 ± 0.16	N	N	4.7
166.....	212	18 02 30.37	22 59 29.0	135	57	8.78 ± 2.43	2.26 ± 0.32	3.88 ± 1.21	0	-0.19 ± 0.09	YSO	U	0.62
170.....	211	18 02 30.93	23 02 35.6	73	21	4.29 ± 1.95	1.27 ± 0.30	3.37 ± 1.73	68	-0.79 ± 0.15	N	Y	0.33
194.....	291	18 02 32.75	23 04 21.0	74	14	5.71 ± 2.18	1.25 ± 0.32	4.56 ± 2.08	2	-0.58 ± 0.13	(YSO)	[Y]	0.34
211.....	72	18 02 34.51	22 59 37.9	312	107	9.98 ± 2.55	2.77 ± 1.69	3.60 ± 2.38	43	-0.47 ± 0.06	Y	[Y]	1.1
237.....	29	18 02 38.85	22 50 06.0	81	13	5.57 ± 2.20	1.79 ± 0.35	3.12 ± 1.38	2	0.24 ± 0.09	(YSO)	N	6.32
246.....	63	18 02 40.42	22 57 53.3	58	23	4.37 ± 1.93	1.01 ± 0.28	4.31 ± 2.25	57	-0.86 ± 0.17	Y	[Y]	0.25
256.....	125	18 02 42.36	23 04 35.7	72	13	13.82 ± 4.52	1.55 ± 0.34	8.90 ± 3.51	0	-0.17 ± 0.11	N	N	0.33
283.....	76	18 02 49.16	22 59 45.4	120	27	9.46 ± 2.53	2.01 ± 0.33	4.72 ± 1.48	3	-0.32 ± 0.10	YSO	[Y]	0.55
285.....	25	18 02 49.36	22 48 32.5	93	10	10.05 ± 2.80	2.71 ± 0.44	3.70 ± 1.19	2	0.11 ± 0.07	N	N	6.2

NOTE.—Units of right ascension are hours, minutes, and seconds, and units of declination are degrees, arcminutes, and arcseconds.

[a] X-ray source numbers are from Table 1, and components A–D of HD 164492 and TC 1 and TC 4 (massive protostellar cores from Cernicharo et al. 1998) are in parentheses. Wavelet ID is the source number identified by wavelet analysis.

[b] The net counts and detection signal-to-noise ratio obtained from wavelet analysis.

[c] The count rate at the maximum count in the bin and at the minimum count in the bin (see the text for details); the ratio is the ratio between the two.

[d] Probability of constancy, which is estimated using the χ^2 test.

[e] Hardness ratio: Spectral hardness ratio = $(H-S)/(H+S)$, where H and S are the count rate for hard (2–8 keV) and soft (0.5–2 keV) bands, respectively.

[f] TTS and YSO are identified using the *JHK* color diagram (details are described in Rho et al 2001). Y: 2MASS detection. N: 2MASS nondetection. The identification with the parentheses is uncertain classification because of uncertain 2MASS photometry.

[g] Optical counterparts. Y: detection; the sources in the Guide Star Catalog are in brackets. N: nondetection. U: uncertain.

[h] The values 14×10^{31} and 6×10^{31} ergs s^{-1} are soft and hard components, respectively, for the CD–C2 blend spectrum.

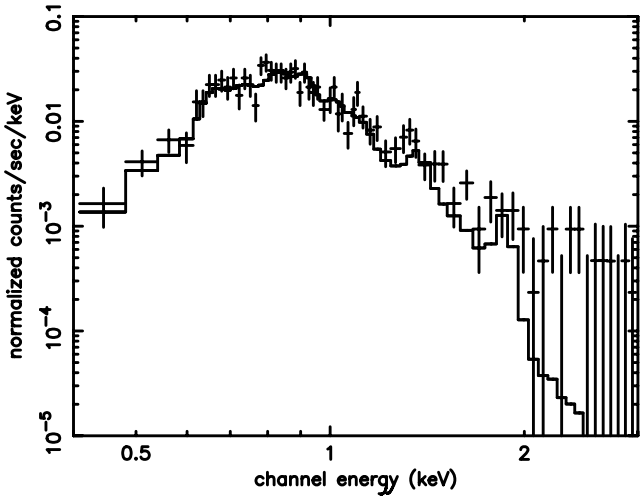

FIG. 3*a*

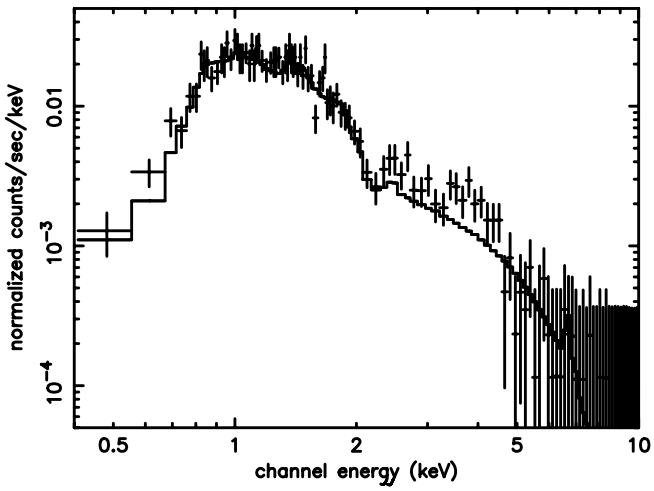

FIG. 3*b*

FIG. 3.—X-ray spectra of (*a*) the HD 164492 A O7.5 III star and (*b*) the HD 164492 CD blend B/Be stars.

similar to the X-ray temperatures of other single massive stars (Corcoran et al. 1994; Moffat et al. 2002). Although some of the luminosity may be due to an unresolved low-mass companion such as a T Tauri star, which could be responsible for the variability, the low temperature obtained from the spectral fit is largely consistent with a single massive star. Assuming a bolometric luminosity of $L_{\rm bol} \sim (0.5\text{–}1.6) \times 10^{39}$ ergs s^{-1}, the ratio of X-ray to bolometric luminosity is $-7.76 < \log L_{\rm X}/L_{\rm bol} < -7.25$, which is smaller than the canonical value, $L_{\rm X}/L_{\rm bol} \approx -7$, but is within the scatter (Berghöfer et al. 1996). The lack of high-temperature X-ray emission in HD 164492A suggests that a magnetically confined wind shock has not developed in the O star of HD 164492A, as has been suggested in other variable O stars showing high-temperature X-ray emission (such as θ Ori A, C, and E; Schulz et al. 2001). Similarly, the lack of hard emission in HD 164492A also suggests that colliding wind emission (as considered in Rho et al. 2001) is not important. X-rays from HD 164492A are likely produced by shocks distributed through the star's massive stellar wind. The variability may be from instabilities within a radiatively driven wind (Lucy & White 1980; Feldmeier et al. 1997), but if so, the rapid timescale of the changes (~2 hr) suggests that the X-ray emission is dominated by a small number of strong shocks rather than a large distribution of weak shocks.

3.2. *HD 164492C*

We also modeled the extracted spectrum from source C, which is blended with the unidentified X-ray source to the northwest (source 91: component C2), which is barely resolved from source C. Component D, a Be star, is not identified as a source by wavelet analysis; however, there is some faint X-ray emission coinciding with the Be star, as shown in Figure 2. Component C2 (source 91) shows variability, and the light curve is shown in Figure 4. The best two-temperature absorbed thermal fit in Figure 3*b* has $N_{\rm H}(1) = 7.8^{+5.2}_{-4.8} \times 10^{21}$ cm^{-2} and a temperature of $kT_1 = 0.6 \pm 0.4$ keV, and $N_{\rm H}(2) = 1.6(^{+4.4}_{-1.1}) \times 10^{21}$ cm^{-2} and a temperature of $kT_2 = 5.9(^{+\infty}_{-3.4})$ keV. The luminosity of soft and hard components are 1.4×10^{32} and 6×10^{31} ergs s^{-1}, respectively. The lower absorption $N_{\rm H}(1) = 1.6 \times 10^{21}$ cm^{-2} is comparable to the optical extinction $A_V = 1$ mag (Kohoutek et al. 1999), suggesting that the wind(s) and the strong ionizing radiation from the O and B stars strip the surrounding materials. The 6 keV component is partially responsible for the spectra seen by *ASCA* (Rho et al. 2001). The X-ray emission from B and Be stars is not well characterized at present, since they are often faint. The $L_{\rm X}/L_{\rm bol}$ ratio is below $10^{-7} \sim 10^{-5}$ for stars of spectral type B1.5 (III–V) and later (Feigelson et al. 2002), and the late-type stars have a luminosity range of 10^{29}–10^{31} ergs s^{-1}. Thus, the observed X-ray emission of 2×10^{32} ergs s^{-1} from the source C blend is difficult to reconcile with emission from a typical B6 V type star or a late-type main-sequence companion star. We extracted separate spectra from both components C and C2, but the spectra could not be distinguished from each other, and additionally we lose the hard component

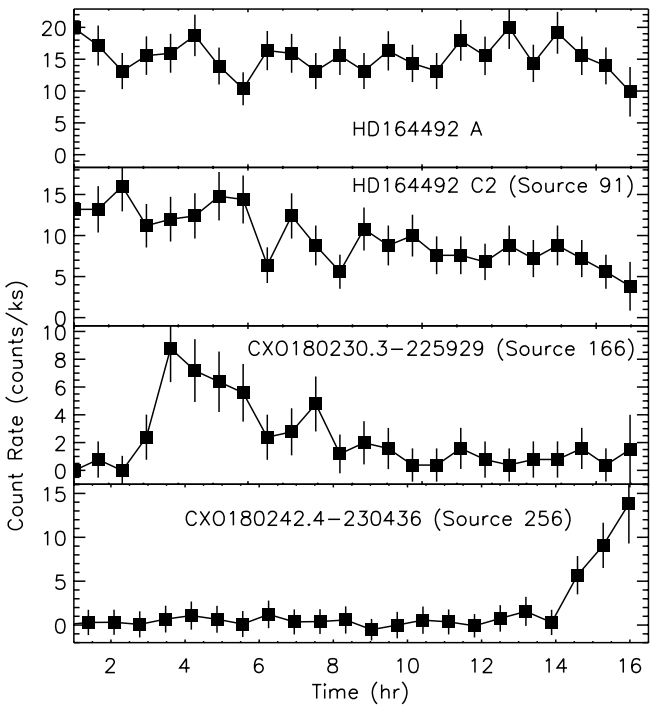

FIG. 4.—Light curves from HD 164492 A and C2 and two PMS stars. The source numbers are marked for each (see Table 1).

emission because of the lack of photon statistics in the hard energy band, although separate light curves show stronger time variability in component C2. The B6 V star is an X-ray source, as shown in Figure 2, and component C2 is a companion candidate, which is also a strong X-ray emitter. It is often suggested that the companions of later B-type stars with strong X-ray emission are PMS stars (Stelzer et al. 2003), which show characteristics of high X-ray luminosities and hard X-rays. The presence of an unidentified X-ray source near the B6 V star and the presence of hard X-ray emission in this system suggest that C2 may be a PMS star. Other possibilities, such as emission from corona of the Herbig Be star or a mechanism related to the proplyds, remain open at this point.

3.3. *HD 164492B*

Component B (source 106) is classified as an A2 Ia (Gahm et al. 1983) or possibly as an A2 III star (Lindroos 1985). A-type stars are not often detected as X-ray sources (Guillout et al. 1999), since they lack subsurface convection zones to power strong magnetic fields and a strong UV flux to power massive stellar winds. This may indicate that this star has a low-mass, X-ray–bright companion or that the spectral type may be incorrect. Its X-ray luminosity is listed in Table 2; we assumed a temperature of 0.15 keV from other A stars (Simon & Drake 1993) and the absorption of 1.6×10^{21} cm^{-2}.

4. PRE–MAIN-SEQUENCE STAR CANDIDATES

We created light curves for each of the detected X-ray sources using a bin length of 2500 s, which gives a total number of 24 bins. We calculated the ratio between maximum count in the highest bin and minimum count in the lowest bin and found that ~40 sources have a ratio greater than 1 after accounting for the errors. If a source was only detected during a flare, we used the mean count rate instead of the minimum count rate.

In Table 2 we list sources in which this ratio is greater than 3 (sources 8, 23, 97, 166, 170, 194, 211, 237, 246, 256, 283, and 285). These should represent the most strongly variable sources. To confirm this variability, we also performed a simple χ^2 test against an assumed constant light curve. The probability of constancy for each source from this test is given in Table 2, for which we used additional binning as needed for each source. Nine sources (sources 23, 91, 97, 166, 194, 237, 256, 283, and 285) in Table 2 are definitely variable (null probability <10%), based on the χ^2 test and our ratio test. We show sample light curves of the variable sources in Figure 4.

We searched for near-infrared and optical counterparts for these variable sources. Unfortunately, no previous optical identification of T Tauri stars exists in the Trifid. The only identified T Tauri stars or young stellar objects are 85 PMS star candidates identified from infrared excesses using 2MASS second release data (Rho et al. 2001). Here we reevaluate the identification of PMS star candidates—TTS or YSO—from near-infrared color-color diagrams using the 2MASS final release data. The final released 2MASS data have improved photometry by allowing multiple components of point-spread function for the blended sources with the improved zero point. Among variable sources in Table 2, only source No. 283 was previously identified as a YSO (Rho et al. 2001), and now sources 23, 97, 166, 194, and 237 are identified as TTS or YSO based on the 2MASS data. We also searched for optical counterparts to these X-ray sources using the Guide Star Catalog (GSC 2.2) and USNO-B Catalog, but since these catalogs do not include any sources near bright optical diffuse emission, we also directly compared the X-ray sources in Table 1 to digital all-sky images (DPOSS). Among the variable sources listed in Table 2, five (sources 97, 166, 237, 256, and 285) have SHR greater than −0.2 (Fig. 1, *blue*).

Sources 8, 23, 194, 211, 246, and 283 have both optical and 2MASS counterparts. These sources are not embedded and thus are likely in the later stage of PMS evolution, possibly Class II or III. Sources 8, 211, and 246 have 2MASS counterparts but are not identified as TTS or YSO from near-infrared colors. They are still likely PMS stars, because the near-IR excess is shown to be time-dependent (Carpenter, Hillenbrand, & Skrutskie 2001). Sources 97, 166, 237, 256, and 285 have no optical counterparts and have SHR greater than −0.2, and the light curve of source 166 is shown in Figure 4. In particular, sources 256 and 285 have neither near-IR nor optical counterparts but exhibit flares in their X-ray light curves, as shown in Figure 4. No radio counterparts are known for these sources. We suggest that these X-ray flare stars are in an early PMS stage (Class I or earlier). Source 211 has sufficient counts for spectral fitting, and the best fit using a one-temperature thermal model yields $N_{\rm H} = 1(<8) \times 10^{21}$ cm^{-2} and a temperature of $kT = 2(>1)$ keV. The inferred X-ray luminosity of 1.1×10^{31} ergs s^{-1} is comparable to those from TTS and YSO (Feigelson & Montmerle 1999) and brighter than those of typical low-mass main-sequence stars (~10^{30} ergs s^{-1}). The sources with flares seem to be found preferentially concentrated along the dust lane and at the edge of the H II region, i.e., along the ionization fronts. This reinforces the conclusion that most of the flaring sources are PMS stars. We estimated the X-ray luminosities of sources 8, 23, 97, 166, 170, 194, 246, 256, and 283, assuming the spectral parameters are the same as those of source 211. For sources 237 and 285, we assumed the spectral parameters are the same as those of the TC 1 source, because their hardness ratios are comparable to that of TC 1.

5. IDENTIFICATION OF X-RAY EMISSION FROM MASSIVE PROTOSTELLAR CORES

We compared the X-ray sources with the known massive star-forming cores detected in the 1300 μm dust continuum map (Lefloch et al. 2001). There are five such cores, four of which are known to have bipolar wings. We detected X-ray emission from TC 1 (source 117) and possibly TC 4 (source 38), two cores with bipolar wings and associated Class 0 candidates (Cernicharo et al. 1998; Lefloch & Cernicharo 2000). The sources associated with both TC 1 and TC 4 are hard X-ray sources (Fig. 1, *blue sources*). Figure 5 shows the positions of the X-ray sources superposed on the 1300 μm dust continuum map. The X-ray source associated with TC 1 has no 2MASS counterpart. However, the X-ray identification of the source associated with the TC 4 core is less clear, because this source is located at the edge of the ACIS field of view, where the width of the point-spread function is ~12″. The TC 4 source coincides with the 1300 μm dust continuum source within 11″–12″ and also has two 2MASS counterparts within 12″. The closest 2MASS source is 2MASS 180212.5−230549, for which *J*-band emission is not detected, and H(=14.8 mag) and K_s(=12.9 mag) magnitudes are contaminated by a nearby star. It is not clear whether this 2MASS source is related to the TC 4 and the X-ray source. TC 4 satisfies the Class 0 definition of André et al. (1993) in terms of its dust temperature (~20 K), the ratio of its submillimeter to bolometric luminosity, and the

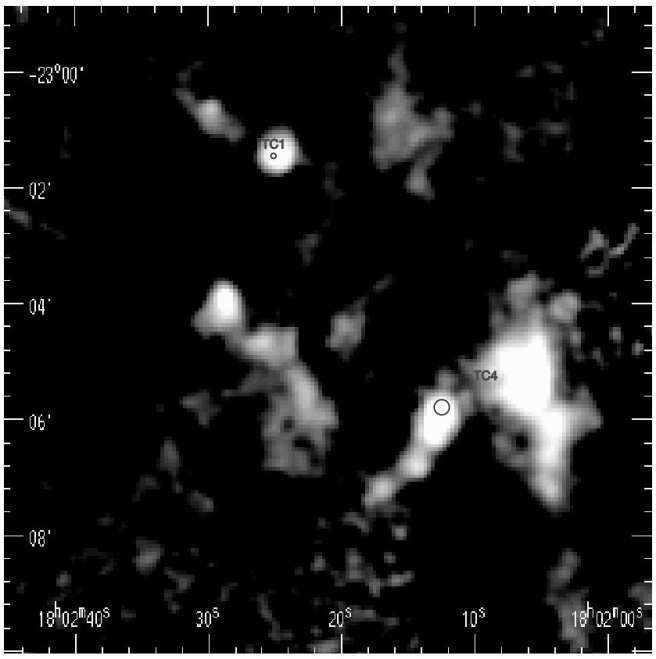

FIG. 5.—1300 μm dust continuum map (Cernicharo et al. 1998), and two X-ray sources coinciding with two of the earliest protostellar cores of TC 1 and TC 4.

presence of a bipolar outflow. An outflow from TC 4 shows a kinematic age of 6.8×10^3 yr and suggests that it is an intermediate- or high-mass object (Lefloch et al. 2002). For TC 1, the SED is not available, so it is not clear whether TC 1 satisfies the Class 0 criteria; however, the object is deeply embedded in a dust core, so it is at least a Class I object and possibly younger than a Class I source.

TC 1 and TC 4 have hardness ratios of 0.24 and 0.67, respectively (see Tables 1 and 2). The source associated with TC 4 is one of the hardest sources in Table 1. These sources are either highly absorbed or have high temperatures. Our analysis of the X-ray spectra of TC 1 and TC 4 shows that the best-fit thermal model parameters are $N_{\rm H} = 6 \times 10^{22}$ cm^{-2}, $kT = 1.7$ keV, and $L_{\rm X} = 4.7 \times 10^{31}$ ergs s^{-1} for the TC 4 source, and $N_{\rm H} = 3.4 \times 10^{22}$ cm^{-2}, $kT = 1.1$ keV, and $L_{\rm X} = 1.9 \times 10^{31}$ ergs s^{-1} for the TC 1 source. The large column densities we derive show that these sources are highly embedded. The only detection of X-ray emission from a Class 0 object until now is a source located in OMC-3 (CSO 6) (Tsuboi et al. 2001). In comparison, the Class 0 source in OMC-3 (CSO 6) has $N_{\rm H} = (1–3) \times 10^{23}$ cm^{-2} and a luminosity of 10^{30} ergs s^{-1}. X-ray emission from Class 0 objects that are in the dynamical infall phase is poorly understood, since so far only a few Class 0 candidates have been identified and their properties are not well constrained. It is unclear whether the X-ray emission is due to solar-type magnetic activities, as in Class I objects. The fact that these two counterparts have high hardness ratios does not support the idea that X-ray emission is from a low-mass companion to the protostellar core. If these objects are accreting, then the X-ray emission may be related to the accumulation and release of angular momentum toward the growing central star by outflow processes.

6. SUMMARY

Young H II regions like the Trifid are rich sources of X-ray emitters. Our *Chandra* images reveal a few hundred X-ray sources including variable and hard sources, along with PMS stars and more evolved OB stars. We summarize our findings here.

1. *Chandra* images show 304 X-ray sources; 30% of the sources are hard, and two-thirds have near-infrared counterparts. The full list of *Chandra* X-ray sources is given in Table 1.

2. The multiple star system HD 164492 is resolved for the first time in X-rays into individual components. X-ray emission is detected from components A, B, and C (a B6 V star), which is blended with an unidentified source in the *Chandra* images. This blend has comparable X-ray brightness to the O star. The O star HD 164492A shows small but significant variability and has a soft spectrum with a temperature of 0.5 keV. The temperature is comparable to those of other single massive stars, and the ratio of X-ray and bolometric luminosities is smaller than the canonical value $L_{\rm X}/L_{\rm bol} \approx -7$; but it is within the scatter of distribution. The lack of any hard component suggests that neither a magnetically confined wind shock nor colliding wind shock is needed to describe the X-ray emission from the O star. The variability of the X-ray emission implies that the emission is produced by a small number of strong shocks in the wind of HD 164492A.

3. The X-ray spectrum from the component C blend requires a two-temperature thermal model with $kT_1 = 0.6 \pm 0.4$ and $kT_2 = 5.9(^{+\infty}_{-3.4})$ keV. The inferred X-ray luminosity is 2×10^{32} ergs s^{-1}. This blend is highly variable in X-rays, which suggests that one of the stars dominates the emission.

4. We found a dozen stars that show evidence of flaring activity, and there could be as many as $\sim$40 variable stars in the full source list. Nine sources (sources 8, 23, 97, 166, 194, 237, 256, 283, and 285 in Table 2) have significant variability based on the χ^2 statistics. We searched for their near-infrared and optical counterparts and found that six stars have both optical and 2MASS counterparts. These sources are likely in later stages of PMS evolution. Four sources that have no optical counterparts and have SHR greater than -0.2 are likely in early stages of PMS, possibly Class I or earlier. There are a few stars with neither near-IR nor optical counterpart whose light curves show strong flares, suggesting that they are very early stage PMS stars.

5. We detected X-ray emission from TC 1 and possibly TC 4, two massive star-forming cores with bipolar wings and associated Class 0 candidates. Both TC 1 and TC 4 show extremely hard X-rays, and their spectra imply very high absorption [$N_{\rm H} = (3.5–6) \times 10^{22}$ cm^{-2}] and high luminosity [$(2–5) \times 10^{31}$ ergs s^{-1}]. Only one other detection of X-ray emission from a Class 0 object has been previously reported. Thus, our two detections imply the second and third X-ray detection of a Class 0 object. It is unclear whether the X-ray emission of these objects is due to solar-type magnetic activities, as in Class I objects. If the X-ray emission is from the accreting stage, the X-ray emission may be related to the competing processes of accumulation of angular momentum toward the growing central star and release of angular momentum by outflow processes.

Of the X-ray sources in the full field, 30% are shown to be hard (SHR > -0.2, *blue*) sources (Fig. 1), and 16% of sources are extremely hard sources (SHR $> +0.2$). A high proportion of these sources are probably PMS stars because they are either highly embedded or have extremely high temperatures. These hard sources, along with the sources near HD 164492C, are responsible for the hard spectra seen by *ASCA*. The

accurate positions from the complete list of the X-ray sources are provided in Table 1. These sources provide an opportunity to identify interesting PMS stars using the multiwavelength follow-up observations, which will help us to further understand the population and evolution of protostellar objects.

Partial support for this work was provided by NASA through *Chandra* grant G02-3095A. J. R. and S. V. R. acknowledge the support of California Institute of Technology, the Jet Propulsion Laboratory, which is operated under contract with NASA.

REFERENCES

Abbott, D. C. 1982, ApJ, 263, 723
André, P., Ward-Thompson, D., & Barsony, M. 1993, ApJ, 406, 122
Berghöfer, T. W., Schmitt, J. H. M. M., & Cassinelli, J. P. 1996, A&AS, 118, 481
Carpenter, J. M., Hillenbrand, L. A., & Skrutskie, M. F. 2001, AJ, 121, 3160
Cernicharo, J., et al. 1998, Science, 282, 462
Chlebowski, T., Harnden, F. R., & Sciortino, S. 1989, ApJ, 341, 427
Corcoran, M. F., et al. 1994, ApJ, 436, L95
Feigelson, E. D., Broos, P., Gaffney, J. A., Garmire, G., Hillenbrand, L. A., Pravdo, S. H., Townsley, L., & Tsuboi, Y. 2002, ApJ, 574, 258
Feigelson, E. D., & Montmerle, T. 1999, ARA&A, 37, 363
Feldmeier, A., Kudritzki, R. P., Palsa, R., Pauldrach, A. W. A., & Puls, J. 1997, A&A, 320, 899
Freeman, P. E., Kashyap, V., Rosner, R., & Lamb, D. Q. 2002, ApJS, 138, 185
Gahm, G. F., Ahlin, P., & Lindroos, K. P. 1983, A&AS, 51, 143
Garmire, G., et al. 2000, AJ, 120, 1426
Guillout, P., Schmitt, J. H. M. M., Egret, D., Voges, W., Motch, C., & Sterzik, M. F. 1999, A&A, 351, 1003
Herbig, G. H. 1957, ApJ, 125, 654
Hester, J. J., et al. 1999, BAAS, 194, 68.10
Imanishi, K., Koyama, K., & Tsuboi, Y. 2001, ApJ, 557, 747
Kaastra, J. S. 1992, An X-Ray Spectral Code for Optically Thin Plasmas (ver. 2.0; SRON-Leiden Internal Report)
Kohno, L., Koyama, K., & Hamaguchi, K. 2002, ApJ, 567, 423
Kohoutek, L., Mayer, Pl., & Lorenz, R. 1999, A&AS, 134, 129
Lada, C. J. 1987, in Proc. IAU Symp. 115, Star Forming Regions, ed. M. Peimbert & J. Jugaku (Dordrecht: Reidel), 1
Lefloch, B., & Cernicharo, J. 2000, ApJ, 545, 340
Lefloch, B., Cernicharo, J., Cesarsky, D., Demyk, K., & Rodríguez, L. F. 2001, A&A, 368, L13
Lefloch, B., Cernicharo, J., Rodríguez, L. F., Miville-Deschenes, M. A., & Cesarsky, D. 2002, ApJ, 581, 335
Lindroos, K. P. 1985, A&AS, 60, 183
Lucy, L. B., & White, R. L. 1980, ApJ, 241, 300
Lynds, B. T., & O'Neil, E. J., Jr. 1985, ApJ, 294, 578
Moffat, A. J., et al. 2002, ApJ, 573, 191
O'Dell, C. R. 2001, AJ, 122, 2662
Raymond, J. C., & Smith, B. W. 1977, ApJS, 35, 419
Rho, J., Corcoran, M. F., Chu, Y.-H., & Reach, W. T. 2001, ApJ, 562, 446
Schulz, N. S., Canizares, C., Huenemoerder, D., Kastner, J. H., Taylor, S. C., & Bergstrom, E. J. 2001, ApJ, 549, 441
Simon, T., & Drake, S. A. 1993, AJ, 106, 1660
Stelzer, B., Huélamo, N., Hubrig, S., Zinnercker, H., & Micela, G. 2003, A&A, 407, 1067
Townsley, L. K., Broos, P. S., Garmire, G. P., & Nousek, J. A. 2000, ApJ, 534, L139
Townsley, L. K., Feigelson, E. D., Montmerle, T., Broos, P. S., Chu, Y.-H., & Garmire, G. P. 2003, ApJ, 593, 874
Tsuboi, Y., Koyama, K., Hamaguchi, K., Tatematsu, K., Sekimoto, Y., Bally, J., & Reipurth, B. 2001, ApJ, 554, 734
Weisskopf, M. C., Brinkman, B., Canizares, C., Garmire, G., Murray, S., & Van Speybroeck, L. P. 2002, PASP, 114, 1